

KLEIYN : A Quadruped Robot with an Active Waist for Both Locomotion and Wall Climbing

Keita Yoneda¹, Kento Kawaharazuka^{1,2}, Temma Suzuki¹, Takahiro Hattori¹, Kei Okada¹

Abstract—In recent years, advancements in hardware have enabled quadruped robots to operate with high power and speed, while robust locomotion control using reinforcement learning (RL) has also been realized. As a result, expectations are rising for the automation of tasks such as material transport and exploration in unknown environments. However, autonomous locomotion in rough terrains with significant height variations requires vertical movement, and robots capable of performing such movements stably, along with their control methods, have not yet been fully established. In this study, we developed the quadruped robot KLEIYN, which features a waist joint, and aimed to expand quadruped locomotion by enabling chimney climbing through RL. To facilitate the learning of vertical motion, we introduced Contact-Guided Curriculum Learning (CGCL). As a result, KLEIYN successfully climbed walls ranging from 800 mm to 1000 mm in width at an average speed of 150 mm/s, 50 times faster than conventional robots. Furthermore, we demonstrated that the introduction of a waist joint improves climbing performance, particularly enhancing tracking ability on narrow walls.

I. INTRODUCTION

In recent years, the development of quadruped robots has been actively conducted [1]–[3]. These robots utilize high-power, low-gear-ratio motors, which enable dynamic motions such as jumping [4]. Furthermore, RL in simulators [5] has facilitated the realization of unified locomotion control that adapts to various ground conditions, including steps and slippery surfaces [6]–[8]. The evolution of both hardware and software has significantly expanded the capabilities of quadruped robots, leading to expectations for various applications. One such application is the automation of material transport and exploration activities in disaster sites and unexplored natural environments [9]. These environments are characterized by large obstacles, such as collapsed buildings and rocks, with significant height variations. However, while quadruped robots have demonstrated effective horizontal locomotion, robots capable of both stable vertical movement and horizontal locomotion have yet to be realized. Although some quadruped robots specialized for vertical movement have been developed, their body structures are highly specialized for climbing, making horizontal movement difficult [10]. To address this limitation, we aim to establish a quadruped robot architecture that integrates both horizontal and vertical locomotion. Specifically, we develop KLEIYN, a quadruped



Fig. 1. Overview of KLEIYN, the quadruped robot with an active waist joint developed in this study. It is capable of both walking and chimney climbing for wide range of walls.

robot capable of both walking and wall climbing, as shown in Fig. 1.

The key contributions of this study are summarized as follows:

- 1) Development of a quadruped robot, KLEIYN, featuring a waist joint and quasi-direct-drive joints.
- 2) Proposal of Contact-Guided Curriculum Learning (CGCL), which gradually modifies the wall-floor transition from a curved surface to a vertical one.
- 3) Realization of chimney climbing on KLEIYN.
- 4) Demonstration of the effectiveness of the waist joint in chimney climbing motion.

II. RELATED WORKS

A. Wall Climbing on Legged Robots

Wall climbing requires the robot to move against gravity, and the robot must support its body using the wall to prevent falling.

Focusing on how the body is supported, wall-climbing legged robots can be classified into two categories: face climbing robots, which climb by gripping the wall, and chimney climbing robots, which climb by pressing against the wall. Examples of face climbing robots include LEMUR 3 [10], SCALER [11], and LORIS [12]. These robots use grippers to grasp wall protrusions, allowing them to support their bodies on vertical surfaces. However, these robots are unable to climb smooth walls that lack graspable protrusions. Additionally, since grasping-based body support is not required for walking on flat ground, the grippers on the feet impede the walking.

¹ The authors are with the Department of Mechano-Informatics, Graduate School of Information Science and Technology, The University of Tokyo, 7-3-1 Hongo, Bunkyo-ku, Tokyo, 113-8656, Japan. [yoneda, kawaharazuka, t-suzuki, t-hattori, k-okada]@jsk.imi.i.u-tokyo.ac.jp

² The author is with the AI Center, Graduate School of Information Science and Technology, The University of Tokyo, Japan.

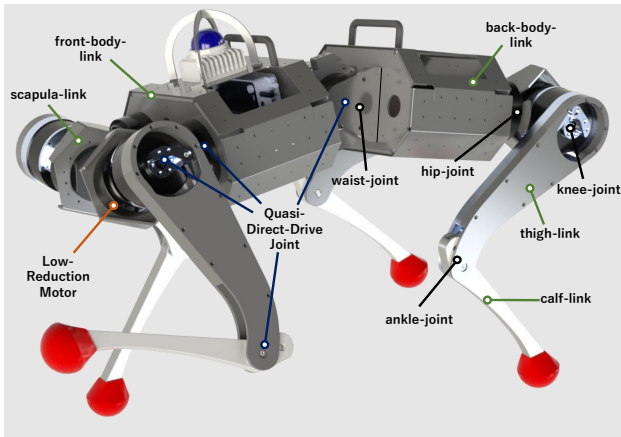


Fig. 2. The design of KLEIYN: Each leg has 3 degrees of freedom (DOF), and a pitch-axis joint with 1-DOF is incorporated into the waist. Each joint is driven by a low-reduction-ratio motor using a quasi-direct drive mechanism.

On the other hand, both chimney climbing and normal locomotion involve pushing against the wall or floor with the feet, making them achievable with the same hardware. Moreover, chimney climbing locomotion can be performed if two opposing walls are present. Therefore, for a quadruped robot aiming to integrate both walking and wall climbing, chimney climbing is a suitable approach. Consequently, this study aims to develop a robot capable of chimney climbing, and the term “wall climbing” in this context specifically refers to chimney climbing.

However, no quadruped robot has been developed that achieves vertical movement by bracing against walls. The only legged robot capable of this is the hexapod robot SiLVIA [13], [14].

SiLVIA is capable of chimney climbing at a speed of 3 mm/s. However, SiLVIA has several limitations. First, its slow leg movements result in a low climbing speed. Second, since its control primarily relies on following a predefined leg trajectory, it lacks the ability to recover from foot slippage. Finally, the absence of joints in the torso prevents it from climbing walls narrower than the width of its body.

B. Locomotion on Legged Robots

In recent years, RL-based control has significantly improved the locomotion performance of quadruped robots. Hwangbo et al. [5] achieved unified locomotion control across various terrains by training a quadruped robot in simulation on flat ground, steps, and slopes. Furthermore, by randomizing model properties and introducing external disturbances, they realized robust control that is resilient to modeling errors and disturbances. Additionally, terrain curriculum improved learning efficiency by gradually increasing the step height during training [15].

In order to learn robust and adaptive control, it is essential to utilize simulation environment. *Teacher-Student Learning* [9], [16] is a learning framework that leverages information available in simulation to improve real-world performance. This approach enables the robot to infer terrain shape and other unobservable factors indirectly from time-series data, allowing for more adaptive control. Furthermore *Asymmetric*

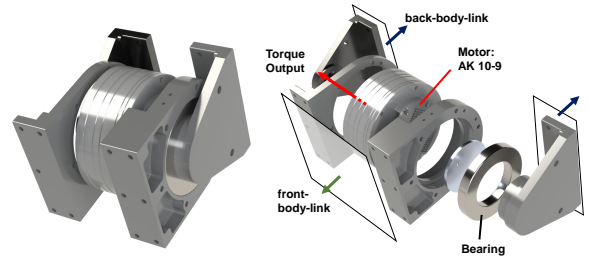


Fig. 3. Design of KLEIYN’s waist joint. The motor output is reduced by a 1:9 gear ratio inside the motor and transmitted to the rotation axis. To maintain rigidity, a bearing is placed on the opposite side of the output shaft to support the load.

Actor-Critic [17], [18] is a method that provides the Critic with observations available only in simulation. By stabilizing value estimation, this method improves overall learning stability. Compared to Teacher-Student Learning, Asymmetric Actor-Critic has the practical advantage of requiring only a single-stage training process, making implementation simpler.

III. DESIGN OF A QUADRUPEd ROBOT KLEIYN WITH AN ACTIVE WAIST

A. Overview of Mechanism

Fig. 2 shows the overall design of KLEIYN. KLEIYN is a quadruped robot with a total of 13 degrees of freedom (DOF), consisting of 3-DOF per leg and 1-DOF in the torso. The robot weighs 18 kg, with a body length of 760 mm and a standing height of 400 mm.

The torso consists of two identical components: the *front-body-link* and the *back-body-link*. Each body link has a box-shaped structure made of four aluminum sheet-metal plates, housing internal components such as the onboard PC and battery. These two body links are connected by the *waist-joint*, which allows pitch-axis bending.

The leg design is based on MEVIUS [19], an open-source metal quadruped robot. Each leg consists of three links: the *scapula-link*, *thigh-link*, and *calf-link*, which are connected by three joints: the *collar-joint*, *hip-joint*, and *knee-joint*. All leg joints are actuated by motors with a 1:10 reduction ratio and a maximum torque of 25 Nm.

A comparison of KLEIYN’s physical parameters with existing quadruped robots is shown in Table I.

TABLE I
COMPARISON BETWEEN KLEIYN AND EXISTING QUADRUPEd ROBOTS

| Robot | Mass | leg length | DOF | Max Torque |
|---------------------|---------|------------|-----|------------|
| ANYmal [1] | 30 kg | 250 mm | 12 | 40 Nm |
| Mini-Cheetah [2] | 9 kg | 200 mm | 12 | 17 Nm |
| MEVIUS [19] | 15.5 kg | 250 mm | 12 | 25 Nm |
| KLEIYN (This Study) | 18 kg | 250 mm | 13 | 25 Nm |

B. Design of Waist Joint

KLEIYN features a 1-DOF rotational joint along the pitch axis, allowing the torso to bend. The design of the waist joint is shown in Fig. 3. The frame is made of machined aluminum parts, and its strength was verified through pre-simulation stress analysis. To enhance rigidity, a double-supported structure is adopted, where a bearing on the

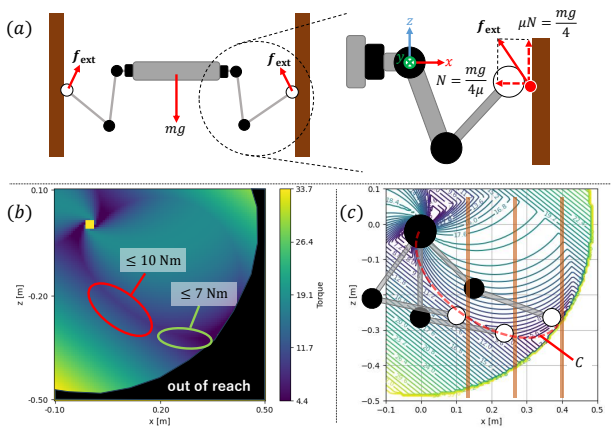


Fig. 4. (a) The dynamic model of the chimney climbing used for torque estimation. The load during bracing is assumed to be evenly distributed across all legs, and the torque calculation is performed for a single leg. (b) The maximum required torque for bracing at the foot position \mathbf{p}_{foot} with external force \mathbf{f}_{ext} , calculated as $\tau_{\text{max}} = \max(\tau_{\{\text{collar}, \text{hip}, \text{knee}\}}) = \max(J(\mathbf{p}_{\text{foot}})^T \mathbf{f}_{\text{ext}})$. (c) Example foot positions using the curve C , where the torque is minimized.

opposite side of the motor output shaft supports the load. For easier sim-to-real transfer in reinforcement learning, the motor output is transmitted to the rotation axis via a low-reduction (1:9) gear in a quasi-direct-drive configuration.

C. Assessment of Motor Torque Suitability

Bracing motion requires greater torque compared to walking. To ensure stable operation, the required torque at each leg joint during bracing was calculated, and motor selection was based on this analysis.

The dynamic model used for the calculation is shown in Fig. 4-(a). Assuming a robot mass of 20 kg while neglecting the leg mass, the force applied to each foot during bracing is considered evenly distributed. The coefficient of friction at the contact point was set to 0.8. Each leg is modeled as a 3-DOF serial linkage, and the joint torques were computed using the Jacobian matrix $J(\mathbf{p}_{\text{foot}})$ at the foot position \mathbf{p}_{foot} as:

$$\boldsymbol{\tau} = -J(\mathbf{p}_{\text{foot}})^T \mathbf{f}_{\text{ext}} \in \mathbb{R}^3. \quad (1)$$

For simplicity, the collar-joint angle is assumed to be constant in calculation of \mathbf{p}_{foot} . The maximum torque values for different foot positions under these assumptions are plotted in Fig. 4-(b).

From the figure, it is observed that despite variations in the distance between the wall and the hip joint, there exists a curve where the maximum torque locally decreases, denoted as curve C . Fig. 4-(c) illustrates curve C along with examples of foot positions following this curve.

As shown in Fig. 4-(b), if the foot position is adjusted along curve C , the maximum torque remains around 10 Nm, even with changes in the wall-to-hip distance. Considering that the load may concentrate when other legs detach from the wall during actual operation, a maximum torque of approximately 20 Nm is deemed sufficient.

Since the waist joint experiences the combined torque from both left and right legs, it requires roughly twice the torque capacity of a single leg joint. Thus, a motor with a

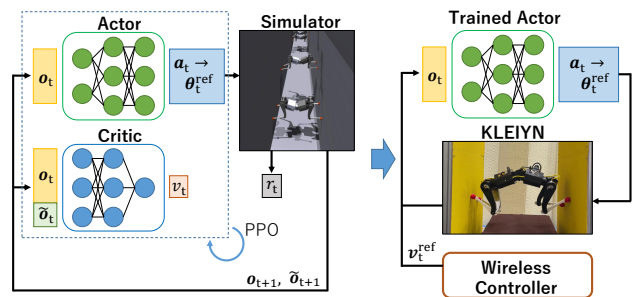


Fig. 5. The training and real-world control framework of KLEIYN. During training, the Actor and Critic are learned using PPO [20] within the Asymmetric Actor-Critic framework. When applying the learned policy to the real robot, only the trained Actor is used, and control is performed to follow the commanded velocity input from the Wireless Controller.

maximum torque of about 40 Nm is adequate for the waist joint. Based on these requirements, the AK 70-10 motor from T-MOTOR, with a maximum torque of 25 Nm, was selected for the leg joints. For the waist joint, the AK 10-9 motor from T-MOTOR, which provides a maximum torque of 48 Nm, was chosen.

IV. REINFORCEMENT LEARNING-BASED CONTROL FOR WALL CLIMBING

A. Control Framework

The control framework of KLEIYN is shown in Fig. 5. During training, two networks are trained: an Actor that outputs actions and a Critic that estimates value functions. When operating the real robot, only the Actor network is used. The Actor outputs scaled target joint angles at a frequency of 50 Hz. These target joint angles are transmitted via CAN communication to each joint motor driver, where they serve as reference values for the internal position control of each motor driver. KLEIYN's sensors include encoders in each motor, a 3D LiDAR (Livox MID-360) mounted on the front-body-link, and an IMU inside the LiDAR. From the encoders, the joint angles $\boldsymbol{\theta} \in \mathbb{R}^{13}$ and joint angular velocities $\dot{\boldsymbol{\theta}} \in \mathbb{R}^{13}$ are obtained. From the IMU, angular velocity $\boldsymbol{\omega} \in \mathbb{R}^3$ and estimated orientation $\mathbf{q} \in \mathbb{R}^4$ are acquired. Additionally, a target velocity $v_z^{\text{ref}} \in \mathbb{R}$ is received from a Bluetooth controller. The point cloud data obtained from the 3D LiDAR is used for SLAM with Fast-LIO [21]. However, the localization results are only recorded and are not used for control.

B. Reinforcement Learning via CGCL for Efficient Learning

1) *Contact-Guided Curriculum Learning (CGCL)*: The key feature of chimney climbing learning is CGCL, where the junction between the wall and the floor gradually transitions from a curved surface to a vertical surface, as shown in Fig. 6. Since this study aims to achieve both horizontal and vertical movement, it is desirable for vertical movement to start from a standing position on the ground. However, transitioning from a standing posture to a bracing posture requires the agent to experience receiving rewards for successful bracing, which can take a considerable amount of time due to the random exploration nature of the learning algorithm. To accelerate learning, we designed an environment where,

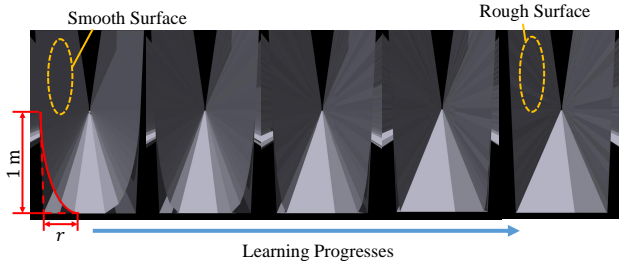


Fig. 6. The terrain used for wall climbing learning. Initially, the floor has a U-shape, which gradually transitions to a vertical surface while the roughness of the wall increases.

in the early stages of training, the terrain naturally induces the agent to experience bracing by randomly moving its feet.

For this purpose, we utilized a curved junction represented by an elliptical arc with a vertical radius of 1.0 m and a horizontal radius of r . By adjusting r , the shape can be made smoother or more vertical. Initially, we set $r = 0.3$ m and gradually reduced it to $r \rightarrow 0.0$ m as training progressed, enabling a smooth transition to fully vertical climbing. Additionally, to ensure adaptability to non-flat wall surfaces, the roughness of the wall was increased as learning progressed.

2) *Learning Environment*: Wall-climbing learning was conducted in a simulation environment using Isaac Gym [22]. To enable the robot to climb walls of various widths, we prepared walls ranging from 900 mm to 1100 mm in width and used them for training. Additionally, to account for modeling errors, we randomized the coefficient of friction of the feet within the range of 0.7 to 0.95 and introduced variations in the mass and moments of inertia of each link. To enhance robustness against external disturbances, we periodically applied random velocity perturbations of 0 to 1 m/s to the front-body-link and continuously applied random external forces and torques. The initial position of the robot was set to a standing posture on the ground ($p_z = 0.4$ m), and the wall height in the simulator was set to 4 m. If the robot successfully climbed the wall ($p_z \geq 3$ m) during training, it was rewarded and reset to the initial position, allowing for more efficient training cycles.

3) *Observation Definition*: The learning algorithm employed Proximal Policy Optimization (PPO) [20], and we introduced an Asymmetric Actor-Critic approach where different information was provided to the Actor and Critic.

The observation for the Actor, denoted as $\mathbf{o}_t = (\mathbf{o}_t)$, and the observation for the Critic, denoted as $\tilde{\mathbf{s}}_t = (\mathbf{o}_t, \tilde{\mathbf{o}}_t)$, are defined as follows:

$$\begin{aligned} \mathbf{o}_t &= (\boldsymbol{\omega}_t, \mathbf{g}_t, \boldsymbol{\theta}_t, \dot{\boldsymbol{\theta}}_t, v_z^{\text{ref}}) \\ \tilde{\mathbf{o}}_t &= (d_t, \mathbf{n}_t, \boldsymbol{\tau}_t, \mathbf{p}_t, \mathbf{q}_t, \dot{\mathbf{p}}_t, \boldsymbol{\omega}_t, \boldsymbol{\rho}, \mathbf{m}, \mathbf{f}_{\text{ext}}, \boldsymbol{\tau}_{\text{ext}}) \end{aligned}$$

Here, $\boldsymbol{\omega}_t \in \mathbb{R}^3$ and $\mathbf{g}_t \in \mathbb{R}^3$ represent the angular velocity vector and the gravity direction vector in the robot's coordinate frame, respectively. $\boldsymbol{\theta}_t \in \mathbb{R}^{13}$ and $\dot{\boldsymbol{\theta}}_t \in \mathbb{R}^{13}$ denote the joint angle vector and joint angular velocity vector, respectively, while $v_z^{\text{ref}} \in \mathbb{R}$ is the reference velocity.

Additionally, $d_t \in \mathbb{R}$ and $\mathbf{n}_t \in \mathbb{R}^3$ represent the distance to the nearest wall and its normal vector from the perspective

of the front-body-link. $\boldsymbol{\tau}_t \in \mathbb{R}^{13}$ represents the joint torque, and $\mathbf{p}_t \in \mathbb{R}$, $\mathbf{q}_t \in \mathbb{R}^4$, $\dot{\mathbf{p}}_t \in \mathbb{R}^3$, and $\boldsymbol{\omega}_t \in \mathbb{R}^3$ represent the global position, orientation, velocity, and angular velocity, respectively. Furthermore, $\boldsymbol{\rho} \in \mathbb{R}^4$ and $\mathbf{m} \in \mathbb{R}^{18}$ represent the friction coefficients at the foot tips and the mass of each link, respectively. $\mathbf{f}_{\text{ext}} \in \mathbb{R}^3$ and $\boldsymbol{\tau}_{\text{ext}} \in \mathbb{R}^3$ denote the external force and external torque applied to the front-body-link.

The origin of the robot, $\mathbf{p} = (p_x, p_y, p_z)$, is placed at the hip joint, and the robot's orientation \mathbf{q} is defined as the average orientation of the front-body-link and back-body-link. In learning, the target velocity v_z^{ref} was randomly assigned within the range of 0.0 m/s to 0.6 m/s.

4) *Reward Definition*: The reward function was designed to encourage the robot's velocity \dot{p}_z to follow the target velocity v_z^{ref} and to maintain a horizontal posture while moving along the wall. The rewards used in training are shown in Table II.

TABLE II
REWARD SETTINGS FOR WALL CLIMBING LEARNING

| Item | Weight | Definition |
|-------------------|--------|--|
| tracking velocity | 3.0 | $f((\dot{p}_z - v_z^{\text{ref}})^2 + \dot{p}_x^2, 0.01)$ |
| collision | -1.0 | $\sum_{i \in P} (\mathbf{f}_i^{\text{contact}} > 0.1)$ |
| climb high | 5 | $p_z > 3$ |
| termination | -500 | $g_z > 0.2$ |
| orientation | -10.0 | $g_x^2 + g_y^2$ |
| rated torques | -3e-2 | $\boldsymbol{\tau} / \boldsymbol{\tau}_{\text{rate}}$ |
| dof acc | -1e-6 | $\ \ddot{\boldsymbol{\theta}}\ ^2$ |
| dof vel | -3e-4 | $\ \dot{\boldsymbol{\theta}}\ ^2$ |
| dof pos limits | -10.0 | $\ \boldsymbol{\theta} - \text{clip}(\boldsymbol{\theta}, 0.8\boldsymbol{\theta}_{\text{min}}, 0.8\boldsymbol{\theta}_{\text{max}})\ $ |
| dof vel limits | -0.1 | $\ \dot{\boldsymbol{\theta}} - \text{clip}(\dot{\boldsymbol{\theta}}, 0.6\dot{\boldsymbol{\theta}}_{\text{min}}, 0.6\dot{\boldsymbol{\theta}}_{\text{max}})\ $ |
| torque limits | -1e-3 | $\ \boldsymbol{\tau} - \text{clip}(\boldsymbol{\tau}, -0.8\boldsymbol{\tau}_{\text{max}}, 0.8\boldsymbol{\tau}_{\text{max}})\ $ |
| center | -0.1 | p_y^2 |
| yaw | -1 | $\boldsymbol{\theta}_{\text{yaw}}^2$ |
| collar angles | -1 | $\sum_{i \in D} \boldsymbol{\theta}_i^{\text{collar}} ^2$ |
| low foot | 0.05 | $\sum_{i \in D} \log(z_i^{\text{foot}} / 0.2)$ |
| base height | 0.4 | $(p_z - 0.6) + 9.0 \min(p_z - 0.6, 0)$ |

Here, $f(x, \sigma) := \exp(-x^2/\sigma) - 0.6x^2$, and the index set $P = \{\text{front-body-link, back-body-link, fl-scapula-link, fr-scapula-link, bl-scapula-link, br-scapula-link}\}$ represents the links penalized for contact. The set $D = \{\text{fl, fr, bl, br}\}$ indicates the four legs. $\mathbf{f}_i^{\text{contact}} \in \mathbb{R}^3$ is the contact force vector applied to each link i . (g_x, g_y, g_z) are the components of the gravity direction vector \mathbf{g} . $\boldsymbol{\tau}_{\text{rate}} \in \mathbb{R}^{13}$ denotes the rated torques for each motor. $\boldsymbol{\theta}_{\{\text{min}, \text{max}\}}$, $\dot{\boldsymbol{\theta}}_{\{\text{min}, \text{max}\}}$, and $\boldsymbol{\tau}_{\text{max}}$ represent the minimum and maximum values for joint angles, joint velocities, and joint torques, respectively. $\boldsymbol{\theta}_{\text{yaw}}$ is the yaw angle of the robot's orientation expressed in Euler angles. Finally, $\boldsymbol{\theta}_i^{\text{collar}} \in \mathbb{R}$ and $z_i^{\text{foot}} \in \mathbb{R}$ denote the collar joint angle and the z-coordinate of the foot position for each leg $i \in D$, respectively.

V. EXPERIMENTS

A. Wall Climbing in Simulation

1) *Chimney Climbing for Wide Range of Walls*: Based on the learned policy, wall climbing motions were performed in the simulator for walls of width 750 mm, 900 mm, and 1100 mm at $v_z^{\text{ref}} = 0.5$ m/s. Fig. 7 shows the climbing motions,

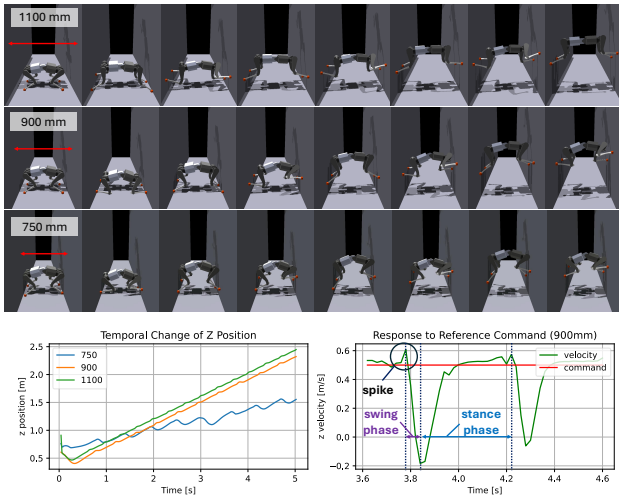


Fig. 7. The wall-climbing experiment in the simulator. Top: climbing motion in the simulator for walls with a width of 750 mm, 900 mm, and 1100 mm at the target velocity $v_z^{\text{ref}} = 0.5\text{m/s}$. Bottom left: Time variation of the z-coordinate for different wall widths. Bottom right: Time variation of vertical velocity for the 900 mm-wide wall.

the variation of the z-coordinate over time, and the change in vertical velocity during the climbing motion on the 900 mm-wide wall.

The climbing motion is realized by alternately executing two phases: the stance phase, where the body is pushed up, and the swing phase, where the legs are lifted. A significant upward velocity is momentarily generated in the vertical direction during the transition from the stance phase to the swing phase, indicating that the robot utilizes recoil when lifting its legs. Although the climbing speed decreases, the robot successfully climbs even the 750 mm-wide wall, which was not included in the training environment. This demonstrates the policy’s generalization capability to unseen wall widths. Furthermore, as discussed in Sec. III-A, KLEIYN has a total length of 760 mm, making it impossible to climb a 750 mm-wide wall without utilizing its waist joint. This indicates that the robot has acquired the ability to climb narrower walls by leveraging its waist joint.

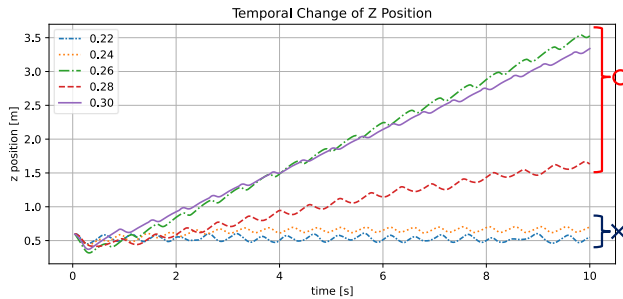


Fig. 8. Comparison of models trained for 20,000 iterations with varying U-shaped parameter r . The graph shows time variation of the z-coordinate when commanding $v_z^{\text{ref}} = 0.5\text{m/s}$ on a 900 mm-wide wall.

2) *Effectiveness of CGCL*: To verify the effect of CGCL, the parameter r , as described in Sec. IV-B.1, was varied, and training was conducted for 20,000 iterations. For evaluation, a 900 mm-wide wall was prepared in the simulator, and an experiment was conducted where $v_z^{\text{ref}} = 0.5\text{ m/s}$ was

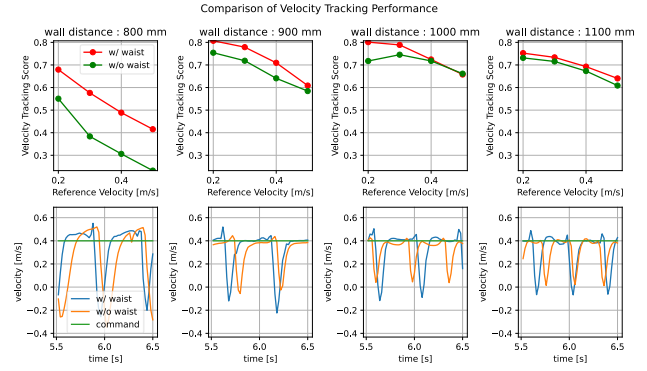


Fig. 9. Comparison of tracking performance with and without the waist joint. Top: Tracking score comparison when commanding a target velocity v_z^{ref} in the range of $0.2 \sim 0.5\text{ m/s}$ for 5 seconds on walls with a width of 800 ~ 1100 mm. Bottom: Comparison of velocity changes when commanding $v_z^{\text{ref}} = 0.4\text{ m/s}$ on walls of width 800 ~ 1100 mm.

commanded. Fig. 8 shows the variation of the z-coordinate over time.

It was observed that the models successfully learned the climbing motion when $r = 0.3, 0.28, 0.26\text{ m}$, whereas they failed to learn proper climbing behavior when $r = 0.24, 0.22\text{ m}$. Furthermore, for values of r smaller than 0.22 m , the models were completely unable to learn the climbing motion. These results suggest that CGCL effectively facilitates the learning of climbing motions and that a threshold exists around $r = 0.25\text{ m}$.

3) The Effect of Waist Joint on Tracking Performance:

To investigate the impact of the waist joint on climbing, we conducted climbing experiments with models both with and without a waist joint. For the model without a waist joint, training was conducted with the same reward and learning algorithm as the model with a waist joint, except that the waist joint was fixed. Fig. 9 shows the tracking score for the target velocity in both models. The four graphs in the top section of the figure compare the tracking scores for walls with width of 800 ~ 1100 mm when commanding $v_z^{\text{ref}} = 0.2 \sim 0.5\text{ m/s}$. The bottom graph compares the velocity changes for walls with a width of 800 ~ 1100 mm when commanding $v_z^{\text{ref}} = 0.4\text{ m/s}$, highlighting the motion differences between the models with and without a waist joint. The tracking score was calculated as the mean value of $f(x, 0.01)$ used in the *tracking velocity* reward function, as defined in Sec. IV-B.4.

The top graphs show that the model with a waist joint achieved higher tracking scores than the model without one. The difference in scores increased as the wall width decreased. In the bottom graph, the model with a waist joint shows a sharper spike in velocity during the transition to the swing phase. This indicates greater utilization of recoil and it enhanced use of recoil likely contributes to improved tracking performance.

These results suggest that using the waist joint improves tracking performance, particularly on narrower walls, and facilitates motion that effectively utilizes recoil.

B. Wall Climbing in the Real World

To verify that the learned wall-climbing behavior could be applied to a real robot, we conducted physical experiments.

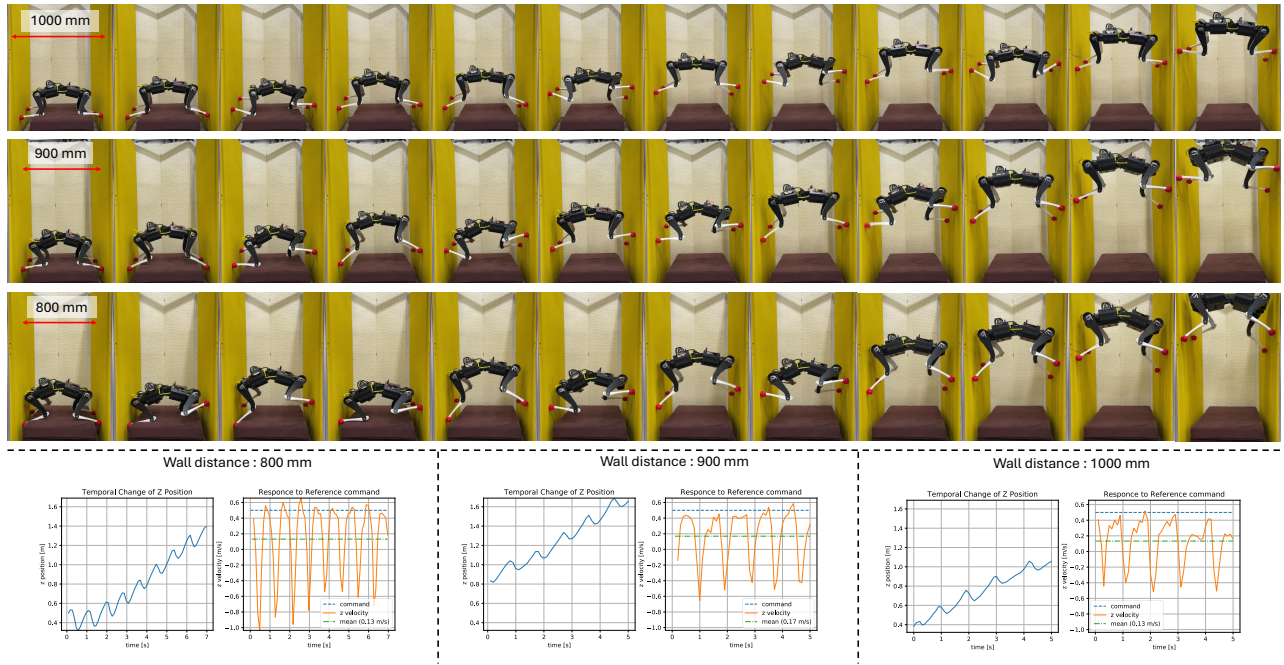


Fig. 10. Wall-climbing experiments on walls with a width of 800 mm, 900 mm, and 1000 mm. The figure shows the climbing motion and the corresponding time-series data of the z-coordinate and vertical velocity for each experiment. In the 800 mm case, the robot achieved a maximum climbing height of 1.0 m with an average climbing speed of 170 mm/s.

We set up a pair of plywood walls facing each other and tested climbing on walls of three different widths: 800 mm, 900 mm, and 1000 mm. The robot was commanded to climb with a target velocity of $v_z^{\text{ref}} = 0.5 \text{ m/s}$. Fig. 10 presents the experimental results, including the climbing motion and the time-series data of the z-coordinate and vertical velocity.

The results demonstrate that the robot successfully climbed in the commanded velocity direction for all wall widths, confirming that the learned model can generalize to different wall widths in the real world. Notably, in the 800 mm case, the robot reached a maximum height of 1.0 m with an average climbing speed of 170 mm/s. This corresponds to climbing 2.5 times its own height and achieving a climbing speed approximately 50 times faster than SiLVIA’s reported average speed of 3 mm/s.

The climbing motion was achieved through alternating stance and swing phases, similar to the simulation experiments. Furthermore, recoil-based movement, observed in the simulation, was also reproduced in the real-world experiments. Additionally, slipping of the legs was frequently observed during the stance phase. In such cases, the robot quickly repositioned the slipped leg and re-established bracing. This suggests that the learned policy is robust against disturbances, such as slipping, through reinforcement learning.

However, differences between the simulation and real-world behavior were also observed. First, the robot failed to climb a 1050 mm-wide wall due to insufficient torque. Additionally, during the swing phase, the downward velocity was larger in real-world experiments than in the simulation. These discrepancies are likely caused by differences in motor torque characteristics and frictional properties between the simulation and the real world. Incorporating these factors

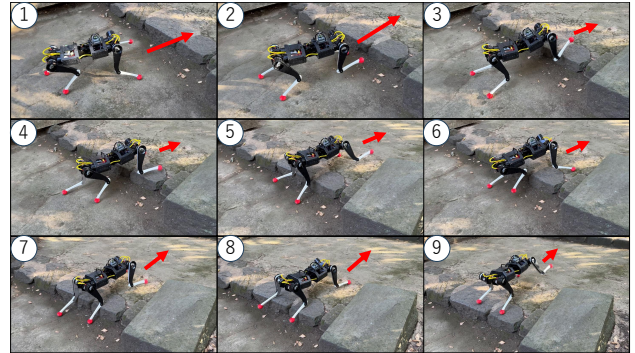


Fig. 11. Outdoor locomotion experiments. The robot successfully traversed a 150 mm step and maintained stability on slippery stones.

into the learning process may further improve performance. Another observed issue was that, despite being commanded only in the vertical direction, the robot moved horizontally and reached the edge of the wall, leading to falls. This is because the current model lacks sensory perception of its environment and cannot detect when it reaches the wall’s edge. This issue could potentially be resolved by integrating environmental sensing, such as LiDAR, to provide the robot with spatial awareness. Lastly, motor overheating posed a challenge for sustained real-world climbing. During climbing, motor temperatures increased, occasionally triggering thermal protection and causing motor shutdowns. The overheating consistently occurred in specific motors, suggesting that optimizing the learning process to distribute motor loads more evenly could help mitigate overheating and extend operation duration.

C. Locomotion in the Real World

To demonstrate that KLEIYN is also capable of locomotion, we modified the wall-climbing reinforcement learning setup by using input commands $\mathbf{v}^{\text{ref}} = (v_x^{\text{ref}}, v_y^{\text{ref}}, \omega_z^{\text{ref}})$ and providing rewards to encourage the robot to follow these reference velocities. The trained locomotion policy was then deployed on the real robot for outdoor walking experiments. Fig. 11 shows the robot's performance in these trials.

The test environment featured a staircase-like terrain with steps of approximately 150 mm in height. KLEIYN successfully ascended and descended these steps using the learned policy. Additionally, while walking on uneven stone surfaces, the robot occasionally experienced foot slippage. In such cases, it was able to quickly recover by repositioning the slipping leg and restoring its posture.

These experiments confirm that the learned locomotion policy is effectively transferable to the real robot. Furthermore, the results demonstrate that KLEIYN can successfully perform both wall climbing and walking, integrating these two modes of locomotion.

VI. CONCLUSION

In this study, we developed KLEIYN, a quadruped robot with an active waist, capable of both walking and wall climbing. For wall climbing, we adopted the chimney climbing and introduced a waist joint to enable adaptation to wide range of walls. Through RL, KLEIYN successfully acquired wall-climbing skills and demonstrated its capability in real-world experiments across 800 ~ 1000 mm of wall widths. To efficiently learn wall-climbing, we introduced a Contact-Guided Curriculum Learning, where the transition between the floor and the wall gradually changed from a smooth curve to a fully vertical surface. This method facilitated efficient learning by guiding the robot to bracing motion. Furthermore, our results demonstrated that the introduction of a waist joint significantly improved tracking performance, particularly on narrow walls. The waist joint allowed the robot to better utilize reactive motions, leading to enhanced adaptability and stability during climbing. This finding highlights the importance of waist joints in quadruped robot design and suggests potential applications beyond wall climbing, such as traversing complex three-dimensional environments.

REFERENCES

- [1] M. Hutter, C. Gehring, D. Jud, A. Lauber, C. D. Bellicoso, V. Tsounis, J. Hwangbo, K. Bodie, P. Fankhauser, M. Bloesch, R. Diethelm, S. Bachmann, A. Melzer, and M. Hoepflinger, "ANYmal - a highly
- [3] "Go1 (Unitree Robotics)," <https://m.unitree.com/go1>.
- [4] G. Bellegarda, C. Nguyen, and Q. Nguyen, "Robust quadruped jumping via deep reinforcement learning," *Robotics and Autonomous Systems*, vol. 182, p. 104799, 2024.
- [5] J. Hwangbo, J. Lee, A. Dosovitskiy, D. Bellicoso, V. Tsounis, V. Koltun, and M. Hutter, "Learning agile and dynamic motor skills for legged robots," *Science Robotics*, vol. 4, no. 26, 2019.
- mobile and dynamic quadrupedal robot," in *Proceedings of the 2016 IEEE/RSJ International Conference on Intelligent Robots and Systems*, 2016, pp. 38–44.
- [2] B. Katz, J. D. Carlo, and S. Kim, "Mini Cheetah: A Platform for Pushing the Limits of Dynamic Quadruped Control," in *Proceedings of the 2019 IEEE International Conference on Robotics and Automation*, 2019, pp. 6295–6301.
- [6] V. Tsounis, M. Alge, J. Lee, F. Farshidian, and M. Hutter, "Deepgait: Planning and control of quadrupedal gaits using deep reinforcement learning," *IEEE Robotics and Automation Letters*, vol. 5, no. 2, pp. 3699–3706, 2020.
- [7] M. Aractingi, P.-A. Léziart, T. Flayols, J. Perez, T. Silander, and P. Souères, "Controlling the solo12 quadruped robot with deep reinforcement learning," *scientific Reports*, vol. 13, no. 1, p. 11945, 2023.
- [8] H. Duan, B. Pandit, M. S. Gadde, B. Van Marum, J. Dao, C. Kim, and A. Fern, "Learning vision-based bipedal locomotion for challenging terrain," in *2024 IEEE International Conference on Robotics and Automation (ICRA)*, 2024, pp. 56–62.
- [9] T. Miki, J. Lee, J. Hwangbo, L. Wellhausen, V. Koltun, and M. Hutter, "Learning robust perceptive locomotion for quadrupedal robots in the wild," *Science Robotics*, vol. 7, no. 62, 2022.
- [10] A. Parness, N. Abcouwer, C. Fuller, N. Wiltsie, J. Nash, and B. Kennedy, "Lemur 3: A limbed climbing robot for extreme terrain mobility in space," in *2017 IEEE International Conference on Robotics and Automation (ICRA)*, 2017, pp. 5467–5473.
- [11] Y. Tanaka, Y. Shirai, X. Lin, A. Schperberg, H. Kato, A. Swerdlow, N. Kumagai, and D. Hong, "Scaler: A tough versatile quadruped free-climber robot," in *2022 IEEE/RSJ International Conference on Intelligent Robots and Systems (IROS)*. IEEE, 2022, pp. 5632–5639.
- [12] P. Nadan, S. Backus, and A. M. Johnson, "LORIS: A lightweight free-climbing robot for extreme terrain exploration," in *IEEE Intl. Conference on Robotics and Automation*, 2024, pp. 18480–18486.
- [13] X. Lin, H. Krishnan, Y. Su, and D. W. Hong, "Multi-limbed robot vertical two wall climbing based on static indeterminacy modeling and feasibility region analysis," in *2018 IEEE/RSJ International Conference on Intelligent Robots and Systems (IROS)*, 2018.
- [14] X. Lin, J. Zhang, J. Shen, G. Fernandez, and D. W. Hong, "Optimization based motion planning for multi-limbed vertical climbing robots," in *2019 IEEE/RSJ International Conference on Intelligent Robots and Systems (IROS)*, 2019, pp. 1918–1925.
- [15] N. Rudin, D. Hoeller, P. Reist, and M. Hutter, "Learning to walk in minutes using massively parallel deep reinforcement learning," in *Proceedings of the 2022 Conference on Robot Learning*, 2022, pp. 91–100.
- [16] J. Lee, J. Hwangbo, L. Wellhausen, V. Koltun, and M. Hutter, "Learning quadrupedal locomotion over challenging terrain," *Science Robotics*, vol. 5, no. 47, 2020.
- [17] L. Pinto, M. Andrychowicz, P. Welinder, W. Zaremba, and P. Abbeel, "Asymmetric actor critic for image-based robot learning," *arXiv preprint arXiv:1710.06542*, 2017.
- [18] I. Radosavovic, S. Kamat, T. Darrell, and J. Malik, "Learning humanoid locomotion over challenging terrain," *arXiv preprint arXiv:2410.03654*, 2024.
- [19] K. Kawaharazuka, S. Inoue, T. Suzuki, S. Yuzaki, S. Sawaguchi, K. Okada, and M. Inaba, "MEVIUS: A Quadruped Robot Easily Constructed through E-Commerce with Sheet Metal Welding and Machining," in *2024 IEEE-RAS International Conference on Humanoid Robots*, 2024.
- [20] J. Schulman, F. Wolski, P. Dhariwal, A. Radford, and O. Klimov, "Proximal policy optimization algorithms," 2017. [Online]. Available: <https://arxiv.org/abs/1707.06347>
- [21] W. Xu and F. Zhang, "Fast-lio: A fast, robust lidar-inertial odometry package by tightly-coupled iterated kalman filter," *IEEE Robotics and Automation Letters*, vol. 6, no. 2, pp. 3317–3324, 2021.
- [22] J. Liang, V. Makovychuk, A. Handa, N. Chentanez, M. Macklin, and D. Fox, "Gpu-accelerated robotic simulation for distributed reinforcement learning," 2018. [Online]. Available: <https://arxiv.org/abs/1810.05762>